ChemComm

Check for updates

Synthesis of core–shell polymer particles in supercritical carbon dioxide *via* iterative monomer addition†

Kristoffer Kortsen, [ID] ‡[a] Morgan Reynolds-Green, [ID] ‡[a] Bradley Hopkins,[ab] Alison McLellan,[a] Matthew J. Derry, [ID] [c] Paul D. Topham, [ID] [c] Jeremy J. Titman, [ID] [a] Daniel J. Keddie, [ID] [a] Vincenzo Taresco [ID] [a] and Steven M. Howdle [ID] *[a]

A new, robust methodology for the synthesis of polystyrene–poly(methyl methacrylate) (PS–PMMA) core–shell particles using seeded dispersion polymerisation in supercritical carbon dioxide is reported, where the core–shell ratio can be controlled predictably *via* manipulation of reagent stoichiometry. The key development is the application of an iterative addition of the MMA shell monomer to the pre-prepared PS core. Analysis of the materials with differing core–shell ratios indicates that all are isolated as single particle populations with distinct and controllable core–shell morphologies.

Polymer particles with core–shell morphologies have a wide range of applications such as surface coatings, printing, catalysis, impact modifiers, pollution control, sensing and drug delivery.[1–4] The interest in core–shell particles derives from their superior properties which arise from the combined characteristics of the core and shell materials.[5]

Core–shell particles are made up of a simple two-component system, consisting of a gas, liquid or solid core encased within a solid shell, typically with a diameter in the nano or micro size range.[5–9] For the synthesis of polymer-based core–shell particles a broad range of monomers have been successfully employed, including (meth)acrylates, styrenes and acrylamides.[5,10]

The synthesis of polymeric core–shell particles in conventional solvents is typically achieved *via* waterborne dispersed phase polymerization processes, such as emulsion, dispersion and precipitation polymerization methods.[5] While these syntheses can be tailored to provide a range of morphologies, isolation of pure polymers by removal of the aqueous

continuous phase is energy intensive and can lead to waste-water contamination.[11–13]

Supercritical carbon dioxide ($scCO_2$) is an alternative to standard solvents, possessing some unique properties; above its critical point (31.1 °C, 73.8 bar) carbon dioxide exhibits a lack of surface tension, enhanced diffusivity, and adjustable density. $ScCO_2$ is also non-toxic and non-flammable. In addition, most vinylic monomers are soluble in $scCO_2$, whereas their polymers are not. This eliminates the need for energy-intensive drying or creation of solvent wastes from precipitation during purification after polymerization; the monomer is simply removed with the $scCO_2$ upon depressurisation.[14] Indeed, these properties of $scCO_2$ have been exploited for the synthesis of polymer materials,[15–20] their impregnation with a range of species,[15,16,21] and the extraction of additives from their internal structure.[22]

As mentioned above, synthesis of core–shell particles in conventional solvents, such as water, has been widely explored. Significant scope however remains to explore their synthesis in $scCO_2$. There are some prior reports in this area, but to date development of a scalable method that delivers control over the shell thickness relative to the core has not been achieved. For example, Cao *et al.* synthesised poly(NIPAM) microgel particles in $scCO_2$ using complex stabiliser molecules that functioned as a stabilising shell.[6,23] While they did produce microgel particles with temperature and pH responsiveness, the shell was in fact the stabiliser from the emulsion system; the overall layer thickness was not demonstrated and true core–shell morphology was not achieved. In a second example, our group previously prepared particles bearing a poly(benzyl acrylate) (PBzA) shell deposited on a poly(methyl methacrylate) (PMMA) core which was successfully synthesised for BzA loadings of 27 wt% with respect to MMA monomer in $scCO_2$. While this initial sample possessed a core–shell morphology, increases in BzA loading resulted in a change of particle morphology rather than increased shell thickness; small internal domains of PBzA were observed surrounded by a continuous PMMA phase. This was attributed to the supercritical fluid's ability to plasticise and swell PMMA, allowing the

[a] School of Chemistry, University of Nottingham, University Park, Nottingham, NG7 2RD, UK. E-mail: steve.howdle@nottingham.ac.uk

[b] Department of Chemical and Environmental Engineering, University of Nottingham, University Park, Nottingham, NG7 2RD, UK

[c] Aston Advanced Materials Research Centre, Aston University, Aston Triangle, Birmingham, B4 7ET, UK

† Electronic supplementary information (ESI) available: Experimental methods and additional characterisation data. See DOI: https://doi.org/10.1039/d3cc04969h

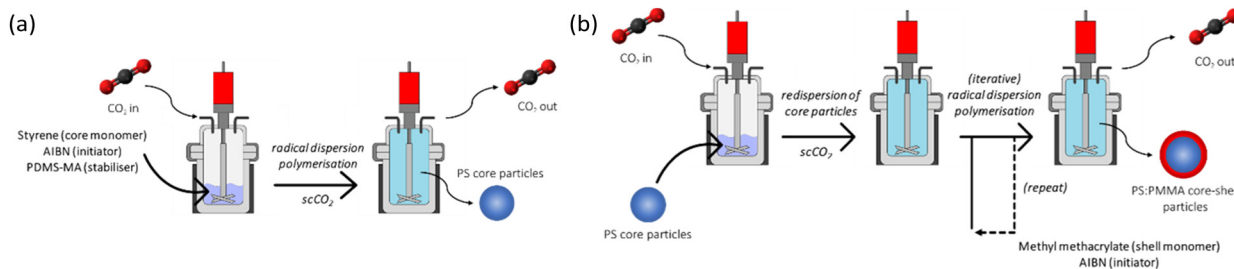‡ These authors contributed equally.

Fig. 1 Reaction schematic of (a) PS core and (b) PMMA shell syntheses in supercritical CO_2 in a high-pressure autoclave.

increasingly more abundant PBzA monomer to permeate into the intended core phase.[24]

Herein, we report a new method, based on seeded dispersion polymerisation, to prepare polymer-based particles with tailored core–shell morphologies, using PS and PMMA as exemplar polymers, where the core–shell ratio can easily be varied by simple manipulation of the reaction conditions, as illustrated by the preparation of particles with core–shell mass ratios of 1:1, 1:2, 1:4, and 1:8. Key to this new methodology is iterative addition of the MMA monomer to the preprepared PS core. This ensures polymerisation occurs on the preformed PS-core particles,§[25,26] preventing secondary nucleation and the formation of unwanted PMMA particle byproducts.

Brief details of the syntheses are provided below (see ESI† for further details). Firstly, the PS core was synthesised via radical polymerisation (RP), using AIBN initiator and PDMS-MA stabiliser in scCO₂ at 65 °C and 245 bar for 24 hours (Fig. 1(a)). The synthesised polystyrene was re-dispersed in scCO₂ at 65 °C and 245 bar for 15 hours, after which stock solutions of AIBN in MMA were injected into the PS suspension. Successive AIBN-MMA injections (i.e. iterative monomer addition) were carried out at 4 hour intervals (Fig. 1(b)). It is necessary to allow the complete polymerisation and hence consumption of the previously injected AIBN-MMA prior to carrying out subsequent injections; excess MMA with respect to preformed particles favours the formation of additional discrete PMMA particles (see Fig. S1, ESI†).

^{1}H NMR (see Fig. S2, ESI†) determined that monomer conversion during PMMA shell synthesis was high (>93%) in all cases (see Table 1). Additionally, ^{1}H–^{13}C CP-MAS NMR analysis of dried particles demonstrated an increase in

PMMA-shell derived signals relative to PS-core signals, consistent with the targeted mass ratios (see Fig. 2(a)).

Scanning electron microscopy (SEM) and dynamic light scattering (DLS) illustrated that relatively uniform particles that were larger than the initial PS core particles had been produced, and that the diameter predictably increased with an increasing MMA monomer feed (see Table 1 and Fig. 2(b)–(f)). A simple predictive model was devised to calculate the diameter of the various core–shell particles, based on assumptions of perfect sphere growth and a consistent density throughout both phases of the particles (see Scheme S1, ESI†). Close agreement between this predictive model and experimentally obtained diameters by SEM and DLS further confirm formation of the desired core–shell morphology (see Table 1 and Fig. S3, ESI†). Additional corroboration of this morphology by small angle X-ray scattering (SAXS) was attempted at diamond light source,[28] however there was insufficient scattering length density contrast to discern the shell thickness (see Fig. S4, ESI†).

Thermal properties of the core–shell particles were analysed by differential scanning calorimetry (DSC) and dynamic mechanical analysis (DMA). DSC indicated that both PS and PMMA were present in the final product, as their respective glass transition temperatures (T_gs) could be observed, ~95 °C for PS and ~125 °C for PMMA (see Fig. S5, ESI†). DMA analyses illustrated a dual transition in the stiffness of the core–shell particles, indicating both polymers were present in different phases (see Fig. 3(a)). To verify this dual transition was the result of the desired core–shell morphology, the materials were compared to physical, unprocessed blends of PS and PMMA particles, prepared at the same mass ratios.¶ Indeed, DMA traces indicated the thermal properties of core–shell particles

Table 1 Characterization data for PS–PMMA core–shell particles prepared in supercritical CO_2

Entry	PS:PMMA mass ratio		MMA conv.^{b} (%)	M_n^c (kDa)	$Đ^c$	d_{SEM}^d (nm)	σ_d^d (nm)	d_{DLS}^e (nm)	PDI^e	$d_{calc.}^f$ (nm)	$T_{g,DSC}$ (°C)		$T_{g,DMA}$ (°C)	
	Targeted	Experimental^a									PS	PMMA	PS	PMMA
1	PS core	—	—	17	2.9	373	77	356	0.146	256	99	—	103	—
2	1:1	1:1.0	93	36	2.4	470	136	401	0.307	448	93	120	108	124
3	1:2	1:1.9	98	40	2.8	509	179	486	0.303	513	99	122	108	120
4	1:4	1:3.7	98	44	2.1	641	160	552	0.361	608	—^{g}	120	108	128
5	1:8	1:8.4	99	50	2.0	736	173	740	0.750	740	—^{g}	120	108	128

^{a} Calculated from ^{1}H NMR and polymer densities (ρ_{PS} = 1.05; ρ_{PMMA} = 1.19).[27] ^{b} Calculated from ^{1}H NMR. ^{c} From GPC analysis (THF eluent, PMMA standards). ^{d} Average diameter (d_{SEM}) and standard deviation of diameter (σ_d) of particles from SEM analysis. ^{e} Average diameter (d_{DLS}) and polydispersity index (PDI) of particles from DLS. ^{f} Calculated theoretical diameter obtained from a predictive model (see ESI for more information). ^{g} T_g transition not observed due to low relative content of PS.
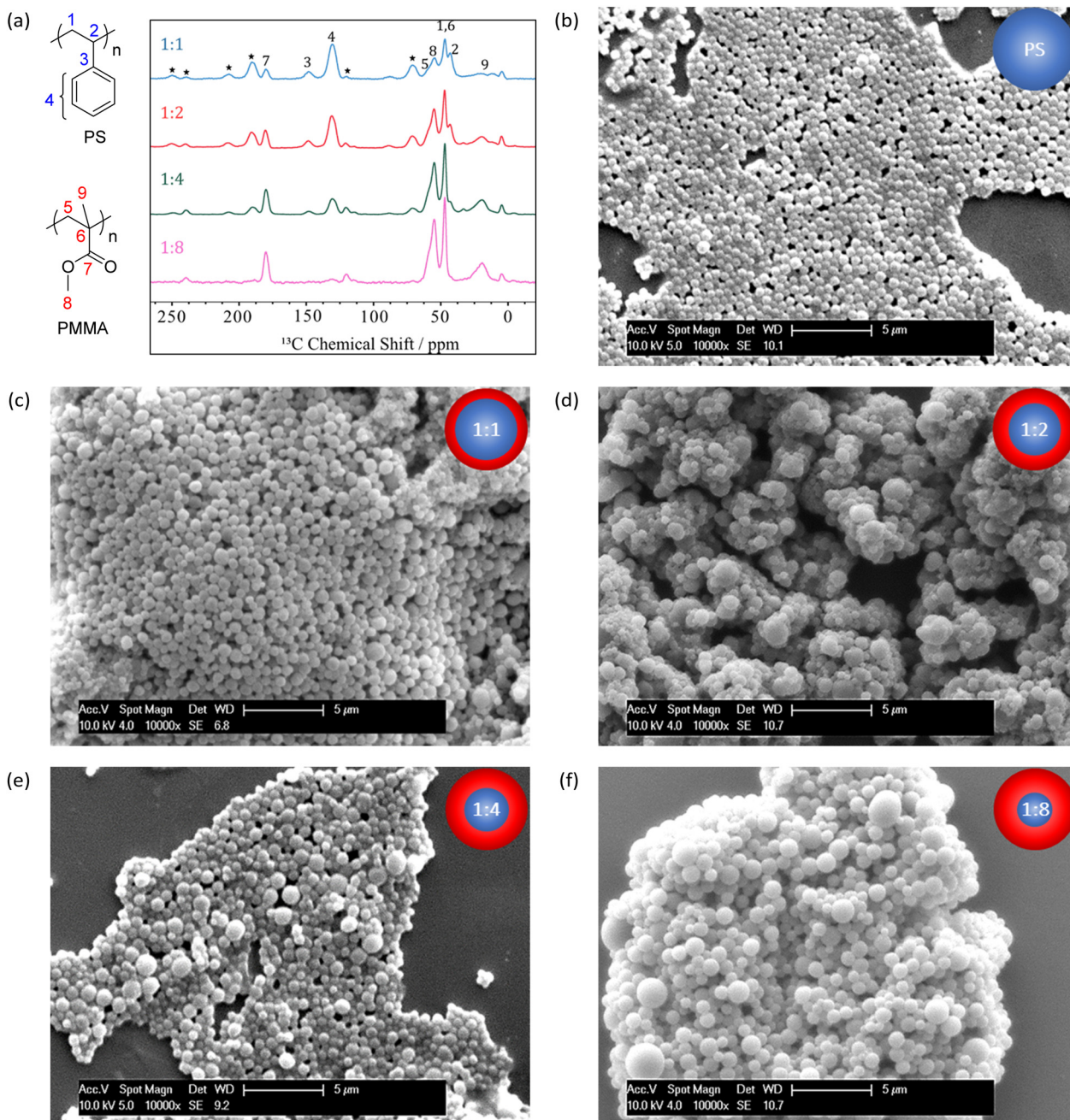
Fig. 2 (a) ^{1}H–^{13}C CP-MAS spectra of PS–PMMA core–shell polymers with PS : PMMA ratios of 1 : 1, 1 : 2, 1 : 4 and 1 : 8 (note: spinning sidebands marked with *, inset shows numbering of ^{13}C assignments), and SEM micrographs of (b) PS particles (core), and PS–PMMA core–shell particles with targeted mass ratios of (c) 1 : 1, (d) 1 : 2, (e) 1 : 4 and (f) 1 : 8.

differ from those of the physical blends. The T_gs of components within the core–shell systems were found to converge, presumably due to molecular interactions at the interface. As expected, the blends displayed discrete T_gs of the individual components (see Fig. S6, ESI†).

To obtain further evidence of core–shell morphology, the particles were viewed by transmission electron microscopy (TEM). The particles were stained with ruthenium tetroxide $(RuO_4)^{29}$ which provides clear contrast between the PS core and PMMA shell, due to interaction of RuO_4 with the aromatic rings of PS (see Fig. 3(b)).

This communication reports the first successful synthesis of core–shell particles in supercritical carbon dioxide, where the core–shell ratio can be controlled predictably. Key to the success of this new methodology is the iterative addition of the MMA during the preparation of the shell to the pre-prepared PS core particles. SEM and DLS demonstrate that there is a single particle population indicating PS and PMMA are co-located within the same particles, whilst DSC, DMA and TEM confirm that two distinct polymer phases were present within the particles. This new method for preparation of
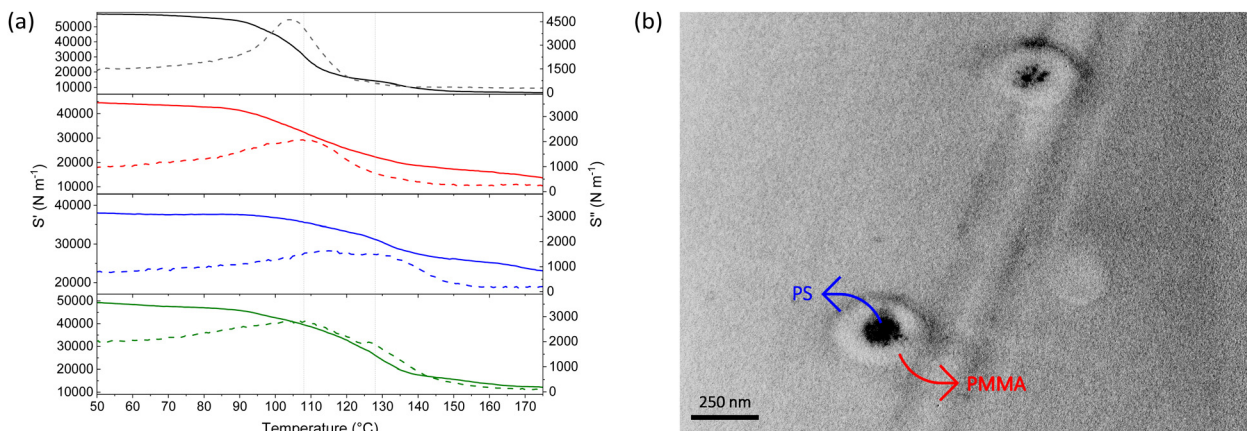
Fig. 3   (a) Storage stiffness (S') (solid lines) and loss stiffness (S'') (dashed lines) for core–shell particles with PS : PMMA targeted mass ratios of 1 : 1 (black lines), 1 : 2 (red lines), 1 : 4 (blue lines) and 1 : 8 (green lines) as function of temperature (note: the guide lines at the T_gs of PS (108 °C) and PMMA (124 °C)), and (b) labelled TEM micrograph of the PS–PMMA core–shell particles with targeted mass ratios of 1 : 1 (note: the PS core has been selectively stained with RuO_4 vapour to show the core–shell morphology).

tailored core- shell materials opens up a route to the preparation of bespoke particles that could be used for a broad range of applications. Importantly, the exploitation of $scCO_2$ as a solvent delivers a greener process than conventional methods, eliminating some chemical hazards and minimizing the energy requirements for product isolation and purification.

Conflicts of interest

There are no conflicts to declare.

Notes and references

§ Due to the low solubility of PMMA in $scCO_2$, polymerisation of MMA is known to (predominantly) occur in the particle (dispersed) phase. See ref. 25 and 26 for more details.
¶ The PMMA particles used in the physical blends were prepared analogously to the PS particles in $scCO_2$ (see ESI†).

1 C. D. Jones and L. A. Lyon, *Macromolecules*, 2003, **36**, 1988–1993.
2 J. S. Downey, R. S. Frank, W.-H. Li and H. D. H. Stöver, *Macromolecules*, 1999, **32**, 2838–2844.
3 N. Sasa and T. Yamaoka, *Adv. Mater.*, 1994, **6**, 417–421.
4 A. K. Khan, B. C. Ray and S. K. Dolui, *Prog. Org. Coat.*, 2008, **62**, 65–70.
5 R. A. Ramli, W. A. Laftah and S. Hashim, *RSC Adv.*, 2013, **3**, 15543–15565.
6 L.-Q. Cao, L.-P. Chen, P.-Y. Cui and J.-D. Wang, *J. Appl. Polym. Sci.*, 2008, **108**, 3843–3850.
7 X. Fu, L. Bao, J. Lei and J. Wang, *J. Vinyl Addit. Technol.*, 2016, **22**, 452–459.
8 J.-S. Lee and F.-C. Chang, *Polym. Eng. Sci.*, 2004, **44**, 1885–1889.
9 W. Schärtl, *Adv. Mater.*, 2000, **12**, 1899–1908.
10 B. R. Saunders and B. Vincent, *Adv. Colloid Interface Sci.*, 1999, **80**, 1–25.
11 S. Kirsch, A. Doerk, E. Bartsch, H. Sillescu, K. Landfester, H. W. Spiess and W. Maechtle, *Macromolecules*, 1999, **32**, 4508–4518.
12 J. Yang, Y. Mu and X. Li, *Mater. Lett.*, 2022, **322**, 132493.
13 L. Y. Wang, Y.-J. Lin and W.-Y. Chiu, *Synth. Met.*, 2001, **119**, 155–156.
14 J. L. Kendall, D. A. Canelas, J. L. Young and J. M. DeSimone, *Chem. Rev.*, 1999, **99**, 543–564.
15 R. R. Larder, E. Krumins, P. L. Jacob, K. Kortsen, R. Cavanagh, L. Jiang, C. Vuotto, I. Francolini, C. Tuck, V. Taresco and S. M. Howdle, *Polym. Chem.*, 2022, **13**, 3768–3779.
16 T. M. Bennett, G. He, R. R. Larder, M. G. Fischer, G. A. Rance, M. W. Fay, A. K. Pearce, C. D. J. Parmenter, U. Steiner and S. M. Howdle, *Nano Lett.*, 2018, **18**, 7560–7569.
17 M. Alauhdin, T. M. Bennett, G. He, S. P. Bassett, G. Portale, W. Bras, D. Hermida-Merino and S. M. Howdle, *Polym. Chem.*, 2019, **10**, 860–871.
18 J. Jennings, M. Beija, A. P. Richez, S. D. Cooper, P. E. Mignot, K. J. Thurecht, K. S. Jack and S. M. Howdle, *J. Am. Chem. Soc.*, 2012, **134**, 4772–4781.
19 G. He, T. M. Bennett, M. Alauhdin, M. W. Fay, X. Liu, S. T. Schwab, C.-G. Sun and S. M. Howdle, *Polym. Chem.*, 2018, **9**, 3808–3819.
20 J. Jennings, G. He, S. M. Howdle and P. B. Zetterlund, *Chem. Soc. Rev.*, 2016, **45**, 5055–5084.
21 D. Varga, S. Alkin, P. Gluschitz, B. Péter-Szabó, E. Székely and T. Gamse, *J. Supercrit. Fluids*, 2016, **116**, 111–116.
22 R. M. N. Guerra, M. A. L. Marín, A. Sánchez and A. Jiménez, *J. Supercrit. Fluids*, 2002, **22**, 111–118.
23 L. Cao, L. Chen, X. Chen, L. Zuo and Z. Li, *Polymer*, 2006, **47**, 4588–4595.
24 A. J. Haddleton, T. M. Bennett, X. Chen, R. L. Atkinson, V. Taresco and S. M. Howdle, *Polym. Chem.*, 2020, **11**, 5029–5039.
25 P. A. Mueller, G. Storti and M. Morbidelli, *Chem. Eng. Sci.*, 2005, **60**, 1911–1925.
26 K. Kortsen, H. R. Fowler, P. L. Jacob, E. Krumins, J. C. Lentz, M. R. A. Souhil, V. Taresco and S. M. Howdle, *Eur. Polym. J.*, 2022, **168**, 111108.
27 *Polymer Handbook*, ed. J. Brandrup, E. H. Immergut, E. A. Grulke, A. Abe and D. R. Bloch, John Wiley & Sons, 2005.
28 A. J. Smith, S. G. Alcock, L. S. Davidson, J. H. Emmins, J. C. Hiller Bardsley, P. Holloway, M. Malfois, A. R. Marshall, C. L. Pizzey, S. E. Rogers, O. Shebanova, T. Snow, J. P. Sutter, E. P. Williams and N. J. Terrill, *J. Synchrotron Rad.*, 2021, **28**, 939–947.
29 W. S. J. Li, V. Ladmiral, H. Takeshima, K. Satoh, M. Kamigaito, M. Semsarilar, C. Negrell, P. Lacroix-Desmazes and S. Caillol, *Polym. Chem.*, 2019, **10**, 3116–3126.